Measurement of drug and macromolecule diffusion across atherosclerotic rabbit aorta *ex vivo* by attenuated total reflection–Fourier transform infrared imaging

Francesca Palombo
Charlène B. Danoux
Imperial College London
Department of Chemical Engineering and
    Chemical Technology
South Kensington Campus
London, SW7 2AZ
United Kingdom

Peter D. Weinberg
Imperial College London
Department of Bioengineering
South Kensington Campus
London, SW7 2AZ
United Kingdom

Sergei G. Kazarian
Imperial College London
Department of Chemical Engineering and
    Chemical Technology
South Kensington Campus
London, SW7 2AZ
United Kingdom

Abstract. Diffusion of two model drugs—benzyl nicotinate and ibuprofen—and the plasma macromolecule albumin across atherosclerotic rabbit aorta was studied *ex vivo* by attenuated total reflection–Fourier transform infrared (ATR–FTIR) imaging. Solutions of these molecules were applied to the endothelial surface of histological sections of the aortic wall that were sandwiched between two impermeable surfaces. An array of spectra, each corresponding to a specific location in the section, was obtained at various times during solute diffusion into the wall and revealed the distribution of the solutes within the tissue. Benzyl nicotinate in Ringer's solution showed higher affinity for atherosclerotic plaque than for apparently healthy tissue. Transmural concentration profiles for albumin demonstrated its permeation across the section and were consistent with a relatively low distribution volume for the macromolecule in the middle of the wall. The ability of albumin to act as a drug carrier for ibuprofen, otherwise undetected within the tissue, was demonstrated by multivariate subtraction image analysis. In conclusion, ATR–FTIR imaging can be used to study transport processes in tissue samples with high spatial and temporal resolution and without the need to label the solutes under study. © *2009 Society of Photo-Optical Instrumentation Engineers.* [DOI: 10.1117/1.3174395]

Keywords: mass transport; drug delivery; macromolecule uptake; atherosclerosis; Fourier transform infrared imaging; attenuated total reflection; multivariate analysis.

Paper 09091R received Mar. 15, 2009; revised manuscript received May 11, 2009; accepted for publication May 22, 2009; published online Jul. 20, 2009.

1 Introduction

Mass transport between blood and the arterial wall, and within the wall itself, plays important roles in the maintenance of the wall tissue, which can be up to ∼1 mm thick but is largely avascular. For example, smooth muscle cells within the wall require delivery of small solutes such as oxygen, ions, glucose, and amino acids, and macromolecules such as growth factors and lipoproteins. Imbalances in the transport of such molecules, and particularly in the transport of lipoproteins, have been implicated in the development of atherosclerosis, the underlying cause of most heart attacks and strokes, which is characterized in its early stages by the deposition of lipids within the inner layers of the wall. Supporting this view, areas of the wall prone to atherosclerosis are characterized by an enhanced uptake of macromolecules from plasma.[1] Mass transport is also key to the delivery of drugs to the arterial media, including the antiproliferative drugs released by drug-eluting stents and drugs to control vascular diameter and stiffness through an influence on smooth muscle tone. Consequently, the transport of plasma-borne molecules into and within the arterial wall has been intensively studied, both ex-

perimentally and theoretically, over the past half-century.[2] Studying the diffusion and distribution of macromolecules has generally involved the use of radioactive or fluorescent labels. Much attention has focused on the transport of low density lipoproteins (LDL),[3–7] serum albumin,[8,9] and horseradish peroxidase.[10,11] Similar methods have been used to study the transport and distribution of drugs in the wall.[12–17]

In the present study, we show that arterial wall mass transport can be studied *ex vivo* by Fourier transform infrared (FTIR) spectroscopic imaging using an attenuated total reflection (ATR) approach. No dyes or labels are required since the FTIR spectrum contains the signatures of vibrational modes involving specific functionalities of a molecule. A focal plane array (FPA) detector is combined with an FTIR spectrometer to obtain FTIR spectroscopic images using different ATR accessories.[18–21] Thousands of infrared absorption spectra are acquired simultaneously from different locations along a specimen surface; the sample depth probed by ATR–FTIR imaging is restricted to a few micrometers from the surface of the specimen in contact with the ATR crystal. The distribution of different constituents within a sample can be obtained by analyzing the acquired spectral dataset for different bands in the mid-IR region: qualitative analysis of the FTIR spectrum

---

Address all correspondence to: Prof. S. G. Kazarian, Department of Chemical Engineering and Chemical Technology, Imperial College London, London SW7 2AZ, UK. Tel: +44 (0)20 7594 5574; E-mail: s.kazarian@imperial.ac.uk.

gives information about the state and environment of the molecule, whereas quantitative analysis through the Beer-Lambert law can be performed by assessing the integrated absorbance of the bands. Studying samples containing water or in contact with aqueous solutions can be challenging because of the absorption of infrared radiation by water. However, we have recently demonstrated the applicability of ATR–FTIR imaging to the study of pharmaceutical and biomedical samples in contact with water and imaged the distribution of water within atherosclerotic rabbit abdominal aorta.[20]

Chemical specificity is the major advantage of this analytical tool, allowing a broad range of applications in different fields.[22–31] The high speed of acquisition offered by the FPA detector is also valuable, enabling kinetic (e.g., pharmacokinetic) properties of different materials to be determined and allowing the study of permeation, diffusion, and dissolution.[32–36] The use of ATR–FTIR imaging to study dynamic properties of biomedical systems (e.g., drug release and sorption) is a rapidly developing area with applications ranging from organs, namely skin,[24] hair,[37] to tablet dissolution.[32,35,38]

In our previous work, micro ATR–FTIR spectroscopic imaging was applied to histological sections of the thoracic aorta of cholesterol-fed rabbit in order to map the chemical composition and location in the wall of experimental atherosclerosis and, in particular, to examine the effects of age and dietary L-arginine on lesions around branch ostia.[39,40] Here, we demonstrate that imaging such sections while applying model drugs or albumin to their endothelial surface allows a temporal series of concentration profiles across the wall to be obtained, without the need for radioactive or fluorescent labels. Moreover, spectroscopic imaging in conjunction with multivariate analysis allows simultaneous observation of the distribution, and hence transport, of at least two biomolecules simultaneously.

2 Materials and Methods

2.1 Materials

Benzyl nicotinate ($\geq$98.0% pure) was obtained from Sigma-Aldrich, ibuprofen from Whitehall International, and bovine serum albumin (fatty acid free) from First Link.

2.2 Solutions

Benzyl nicotinate, poorly soluble in aqueous media, was dissolved in Ringer's solution (composition in g/L: NaCl, 9.0; KCl, 0.2; $CaCl_2$, 0.2; $NaHCO_3$, 0.1) at the saturation limit, and the resulting solution was used. Albumin 6% (w/w) was dissolved in phosphate buffered saline (PBS; 0.15M, pH 7.4). Ibuprofen, also sparingly soluble in water, was added to the albumin solution; the supernatant of the drug-saturated solution was used.

2.3 Tissue Samples

Animal procedures complied with the Animals (Scientific Procedures) Act 1986. Immature (2-months old) male New Zealand white rabbits (HSDIF strain, Harlan) were used in this study. They were housed at $18(\pm2)$ °C under a 12-h light cycle and fed 75 g per day of normal chow (9603 TRB Rabbit; Harlan Teklad, Bicester, UK) supplemented for
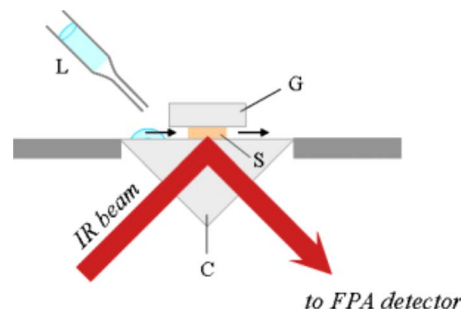

Fig. 1 Schematic diagram of the diffusion experiment using a solution (liquid, L) and a specimen (section of rabbit aorta, S), in contact with the surface of a diamond crystal (C) for ATR–FTIR spectroscopic measurements. A piece of glass slide (G) is placed above the tissue to seal the compartment, and a gentle pressure is applied through an anvil. The solution is added at the endothelial edge of the tissue; the solute then diffuses toward the adventitial edge by permeating the aortic wall. The experiment mimics the diffusion process that brings drugs and solutes from the lumen to the adventitia of the artery.

8 weeks with 1% (w/w) cholesterol (Sigma). The cholesterol was added in ether (inhibitor-free spectrophotometer grade, Sigma), which was then evaporated.

Each rabbit was sacrificed with an overdose of pentobarbital (Euthatal, Rhône Mérieux, iv), and the descending aorta was excised after fixation *in situ* at physiological pressure for 10 min with 10% neutral buffered formalin. A segment of thoracic aorta containing the third pair of intercostal branches was post-fixed for at least 24 h in further formalin solution and then opened along the ventral wall. The segment was immersed in a 2M sucrose solution overnight to inhibit the subsequent formation of ice crystals, before being embedded in Bright cryo-m-bed (Bright Instruments, Huntingdon, UK) and frozen. Longitudinal sections 15 μm thick were cut in a cryostat and mounted on standard microscope slides.

2.4 Spectroscopy

ATR–FTIR images were acquired using a rapid scan Varian system comprising an FTIR spectrometer (Bio-Rad FTS-60A) coupled to a large sample compartment containing a macro-ATR accessory with diamond crystal (Specac Ltd.) and a liquid nitrogen–cooled 64$\times$64 FPA detector. Each image corresponded to a 550$\times$610 μm^2 area of the specimen. Spatial resolution with this experimental setup is about 15 to 20 μm.[41]

Sections of rabbit aorta were soaked with Ringer's solution and gently detached from the microscope slide before being transferred onto the ATR crystal for imaging. A piece of glass slide was placed on top of the section to seal and create a diffusion compartment. Only a low contact pressure was applied, through an anvil, to avoid damaging the tissue; this generally ensured a good contact between specimen and crystal and prevented the leakage of diffusing solution underneath the tissue (see schematic diagram of the experiment in Fig. 1). The evanescent wave from the crystal has a depth of penetration of approximately 2 μm at a wavenumber of 1000 cm^{-1}.

Before each experiment, the tissue sections were rehydrated by applying Ringer's solution and allowing them to equilibrate on the ATR crystal. (Generally 30 min was sufficient.) Rehydration will have further improved the seal be-

tween the section and the glass or crystal. It was monitored by measuring spectroscopic images until no change was observed in the absorbance of water bands between successive snapshots. Solutions of drug or protein were then applied to the endothelial surface of the section, between the glass slide and crystal. Experiments were conducted at least in duplicate.

Varian Resolution Pro 4.0 software was used for acquisition and manipulation of the data. An IR absorption spectrum was obtained for each detector pixel by co-adding 32 interferograms. Spectra were obtained over the range 4000 to 900 cm^{-1} at 4 cm^{-1} resolution with a zero filling factor of 2, achieving a collection time of approximately two minutes per image. For all image measurements, a background was acquired in the absence of a sample.

Each spectroscopic image is a 3-D dataset of absorbance values at various combinations of wavenumber and position in the image plane. The fingerprint region (1800 to 900 cm^{-1}) of the mid-infrared spectrum was analyzed for each detector pixel, and chemical images were generated by integration of characteristic bands contained therein. To calculate the absorbance of each band, a linear baseline was drawn through the troughs either side of the peak, and the absorption profile above this line was integrated with respect to wavenumber.

Multivariate analysis was also performed on an FTIR image of ibuprofen diffusion using ISys 4.0 software. The image measured at the beginning of the experiment, before the application of the drug, was subtracted from the image collected at the end of the experiment to remove the spectral contribution due to the tissue. Factor analysis was employed in the fingerprint region of the resulting dataset; a linear baseline was drawn through the extremes of this spectral range to avoid spurious baseline effects. Selection of relevant factors was based on visual inspection of the score images and loading spectra, as previously described.[40]

3 Results

3.1 *Diffusion of Benzyl Nicotinate*

Benzyl nicotinate in its liquid state readily diffuses across sections of thoracic aorta from cholesterol-fed rabbits (data not shown); however, this process has no *in vivo* relevance. To reproduce a more realistic situation, a saturated solution of benzyl nicotinate in Ringer's solution was applied to the sections. Note that the concentration of benzyl nicotinate at the saturation limit was too low for the drug to be detectable in the FTIR spectrum of the solution.

Figure 2 shows ATR–FTIR images from a representative experiment to assess diffusion across a longitudinal section of rabbit thoracic aorta at a location upstream of the intercostal branch ostium. No atherosclerotic lesion was visible in this region. The images showing the tissue at different times during the experiment are derived from the amide II band (1580 to 1480 cm^{-1}), corresponding mainly to N–H bending of the peptide group [Fig. 2(a)]. The benzyl nicotinate solution was applied to the endothelial edge of the arterial section. The spectroscopic images showing the distribution of the drug at different times during the experiment were obtained using the asymmetric C—O stretching band of the benzyl nicotinate (1294 to 1260 cm^{-1}) [Fig. 2(b)]. The presence of benzyl nicotinate in the tissue was detected a few minutes after the
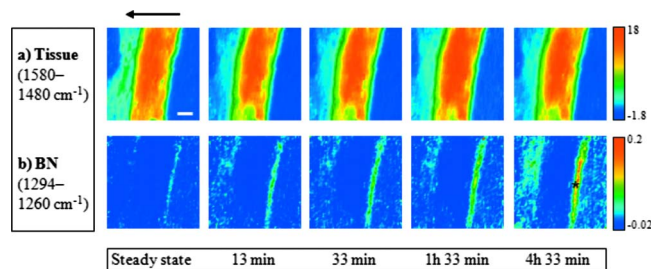

Fig. 2 Spectroscopic images of the diffusion experiment using a benzyl nicotinate–saturated Ringer's solution and a longitudinal section of rabbit thoracic aorta without any lesions. (a) ATR–FTIR images of the tissue at a location upstream of the branch ostium obtained from the spatial distribution of the integrated absorbance of the amide II band, in the range 1580 to 1480 cm^{-1}. No lesion is revealed by integrating between 1760 and 1710 cm^{-1}, in the ν(C=O)$_{ester}$ region. In these images, the outermost media/adventitia layer forms the left edge of the tissue, whereas the endothelium is at the right edge. The intensity scale associated with each image is such that blue and red extremes respectively correspond to low and high absorption values as given by spectral integration; this is directly related to a density scale (Beer-Lambert law). (Scale bar: 100 μm.) (b) ATR–FTIR images of the benzyl nicotinate distribution at this location of the tissue as given by the integrated absorbance of the ν_{asym}(C—O) band in the range 1294 to 1260 cm^{-1}. (The arrow indicates the sense of the diffusion— from the endothelial to the adventitial edge of the aortic wall. The asterisk refers to the pixel-region of the images from which FTIR spectra were extracted.) (Color online only.)

start of the experiment. It penetrated the endothelial surface of the tissue in contact with the drug solution and progressively accumulated within the intima, while the interior of the wall (media) was almost spared. The concentration of drug within the inner wall appears higher than that in the solution in contact with the tissue [see Fig. 2(b)]; hence a partitioning effect of benzyl nicotinate, possibly into lipids that accumulated in the intima during the cholesterol-feeding, seems to have occurred. The increase of band absorbance in the adventitia may reflect seepage of the solution around the section and subsequent entry from the adventitial side. A more likely explanation, however, is that it also results from partitioning, since the adventitia is rich in lipids.

Figure 3(a) shows the evolution of the FTIR spectrum as a function of the time at a pixel within the intima, indicated by the asterisk in Fig. 2. The spectrum of pure benzyl nicotinate is also presented for comparison. The accumulation of the drug into this area of the tissue is indicated by an increase in the asymmetric C—O stretching band. The graph in Fig. 3(b) displays the integrated absorbance of this band for this location as a function of time after the start of the experiment; the drug concentration increases rapidly at the beginning of the experiment and then continues to increase at a less rapid rate.

The diffusion of benzyl nicotinate was also studied across specimens of immature rabbit aorta containing an atherosclerotic lesion (at the downstream margin of the branch ostium). The ATR–FTIR images for this experiment are shown in Fig. 4. Concentration of benzyl nicotinate was observed in the lesion [see Fig. 4(c)], while no permeation of the medial layers of the aortic wall was detected, supporting the idea of partitioning. Note the different scales required in Fig. 2(b) and Fig. 4(c), indicating that the concentration of drug in the le-
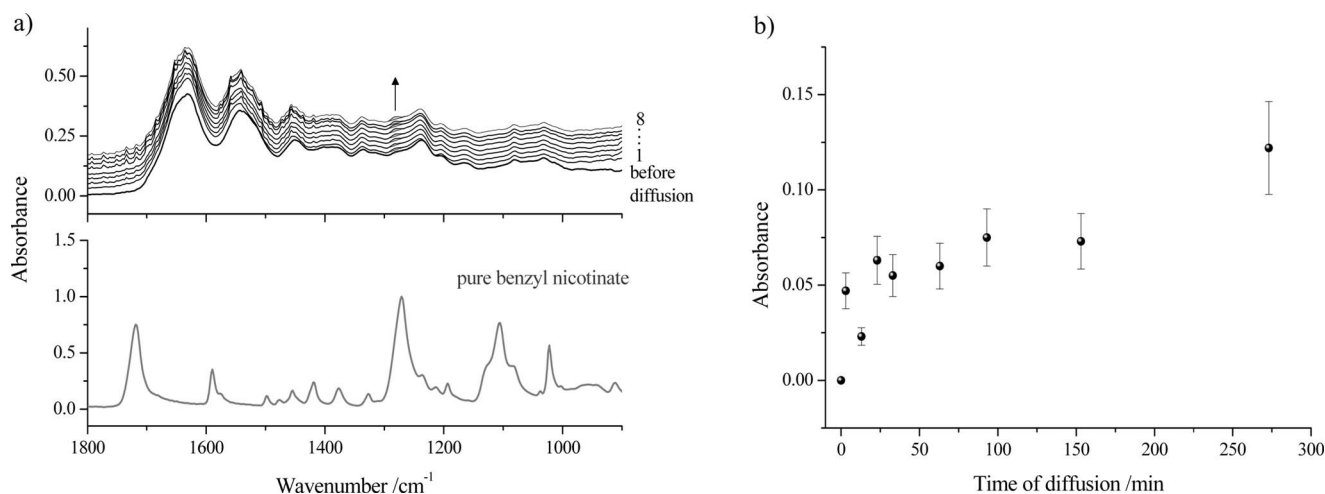
Fig. 3 (a) FTIR spectra extracted from a region within the intima [see asterisk in Fig. 2(a)] at different times after the start of diffusion (from 1 to 8: 3 min to 4 h 33 min). The spectrum of pure benzyl nicotinate is also shown. (The arrow indicates the increase in absorbance of the benzyl nicotinate band in the range 1294 to 1260 cm^{-1}.) (b) Plot of the integrated absorbance of the benzyl nicotinate band in the range of 1294 to 1260 cm^{-1} as a function of time.

sion was more pronounced than that in the inner healthy wall at comparable times.

The spectra corresponding to a single-pixel location within the lesion (asterisk in Fig. 4) show an increase of absorbance of the benzyl nicotinate bands with time [Fig. 5(a)]. The concentration of benzyl nicotinate, expressed by the integrated absorbance of the band in the range 1294 to 1260 cm^{-1}, appeared to increase linearly during the course of the experiment [Fig. 5(b)]. Comparing the plots in Figs. 5(b) and 3(b), confirms that the diffusion and accumulation of benzyl nicotinate within the lesion is higher than in the normal aortic intima.
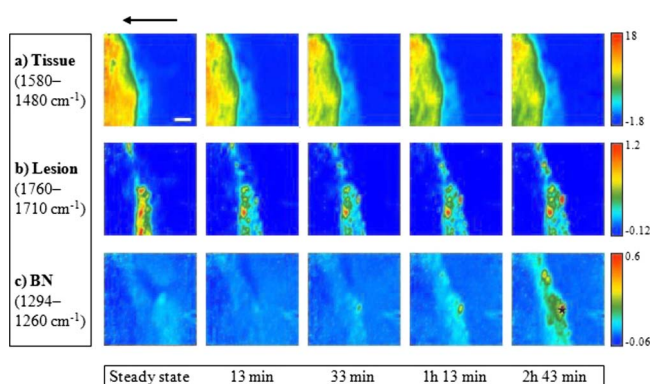

Fig. 4 Spectroscopic images of the diffusion experiment using a benzyl nicotinate–saturated Ringer's solution and a longitudinal section of rabbit thoracic aorta with an atherosclerotic lesion. (a) ATR–FTIR images of the tissue downstream of the branch ostium obtained from the spatial distribution of the integrated absorbance of the amide II band, in the range 1580 to 1480 cm^{-1}. (b) A lesion is revealed by integration of the $\nu(C=O)_{ester}$ band between 1760 and 1710 cm^{-1}. (Scale bar: 100 μm.) (c) ATR–FTIR images of the benzyl nicotinate distribution at this location of the tissue given by integrating the $\nu_{asym}(C-O)$ band, in the range 1294 to 1260 cm^{-1}. (The arrow indicates the sense of the diffusion—from the endothelium to the interior of the aortic wall. The asterisk refers to the pixel-region of the images from which FTIR spectra were extracted.)

3.2 *Diffusion of Ibuprofen-Saturated Albumin*

At saturation, the concentration of ibuprofen in aqueous solution was too low to produce detectable levels of the drug in tissue sections unless albumin was added as a carrier. A solution of ibuprofen and 6% BSA in PBS was used for the representative experiment reported here. As before, the drug solution was applied to the endothelial edge of the aortic tissue. Figure 6 shows spectroscopic images of the diffusion of ibuprofen-saturated albumin across a specimen of rabbit aorta without visible atherosclerotic lesions. The images of the tissue at different times during the experiment were obtained using the amide II band absorbance, in the range 1580 to 1480 cm^{-1} [Fig. 6(a)]. The images showing the distribution of the drug as a function of the time were derived from integration of the ibuprofen band in the range 1294 to 1260 cm^{-1} (C—O stretching (COOH) and O—H bending) [Fig. 6(b)].

Figure 7 shows the evolution of FTIR spectra with time for two locations in the tissue, one in the intima (indicated by an asterisk in Fig. 6) and the other in the media (circle in Fig. 6). For both sites, the fingerprint profile gradually increases in intensity as the diffusion time increases; in particular, the amide I and II band absorbance increases due to the penetration of albumin within the tissue. Note that the spectral evolution is greater in the case of the intima [Fig. 7(a)], which is the part of the tissue directly in contact with the solution, than in the medial layer [Fig. 7(b)]. The plots in Figure 8 show the evolution of the FTIR spectra at the same locations [Fig. 8(a): intima; Fig. 8(b): media] as a function of time after the ibuprofen–albumin solution was removed from the sample compartment. These results demonstrate the reversibility of the transport process.

3.2.1 *Analysis of albumin diffusion*

Spectra were extracted from the ATR–FTIR images described earlier along a horizontal line of the detector array corresponding to a line across the aortic wall [see Fig. 9(b)]. Integration of the spectral region between 1800 and 1480 cm^{-1},
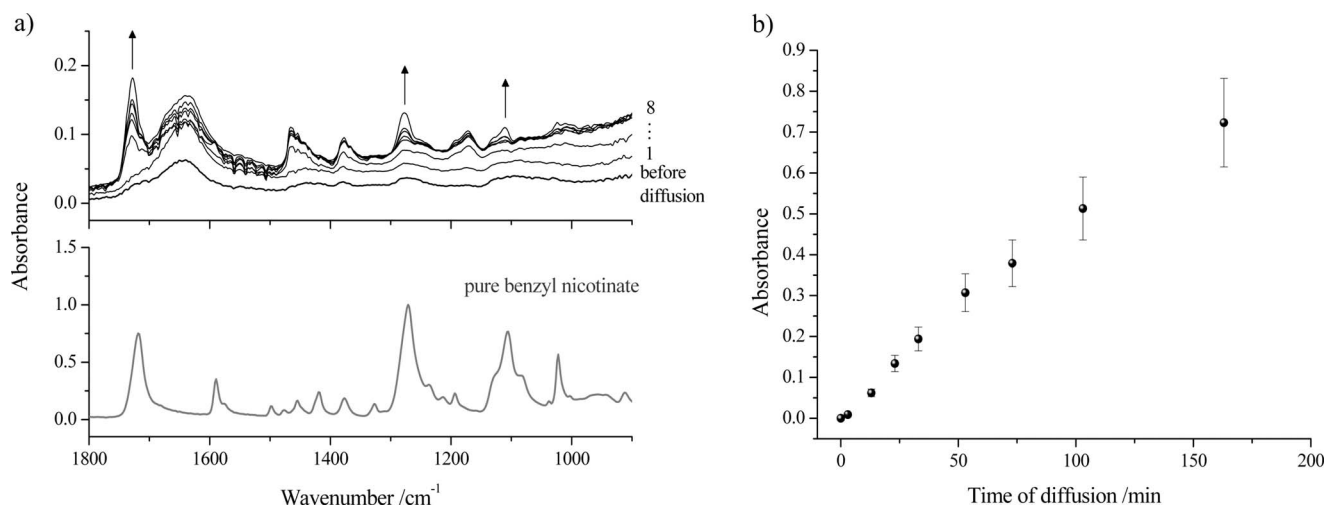
Fig. 5 (a) FTIR spectra extracted from a region within the lesion [see asterisk in Fig. 4(c)] at different times after the start of diffusion (from 1 to 8: 3 min to 2 h 43 min). The spectrum of pure benzyl nicotinate is also shown. (The arrows indicate the increase in absorbance of prominent benzyl nicotinate bands in this spectral region.) (b) Plot of the integrated absorbance of the benzyl nicotinate band in the range 1294 to 1260 cm^{-1} as a function of time.

which corresponds to the amide I and II bands, was performed according to the method in Fig. 9(a). Figure 9(c) shows the transmural concentration profiles for albumin across the artery wall at different times, obtained in this way. (The corresponding absorbance at the start of the experiment was subtracted so that no contribution arose from the tissue itself.) The transmural concentration plots show that the penetration of albumin occurs first in the inner layers of the tissue in contact with the solution (<50 μm thickness). An increase in the albumin content is observed with time, especially within the intima/inner media. Low permeation of the outermost media/adventitia is detected, although an increase in protein levels is observed towards the end of the experiment.
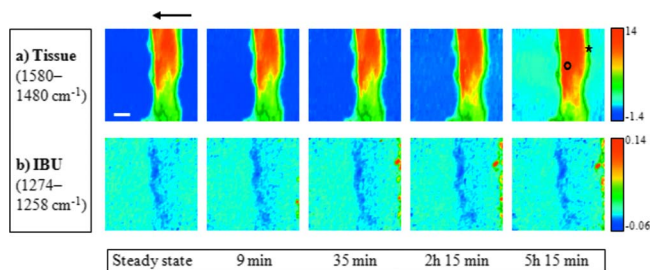

Fig. 6 Spectroscopic images of the diffusion experiment using an ibuprofen-saturated albumin solution (6% in PBS) and a longitudinal section of rabbit thoracic aorta without an atherosclerotic lesion. (a) ATR–FTIR images of the tissue derived from the integrated absorbance of the amide II band, in the range 1580 to 1480 cm^{-1}. The outermost media/adventitia layer is at the left side of the images, whereas the endothelium is at the right side. (Scale bar: 100 μm.) (b) ATR–FTIR images of the ibuprofen distribution given by integration of the band in the range 1274 to 1258 cm^{-1}. Ibuprofen crystals were detected at the right side of the images during the time of the experiment; however, no drug permeation of the aortic wall tissue is revealed here. (The arrow gives the sense of the diffusion. The asterisk and circle indicate the pixel-regions within the intima and media, respectively, from which FTIR spectra were extracted.)

3.2.2 Multivariate image analysis

Factor analysis was applied to the dataset collected at the end of the experiment (315 min), after the dataset for the beginning of the experiment had been subtracted. Two factors were selected, based on the spectral features of the loading spectra and on visual inspection of the score images. The first factor yielded the distribution shown in Fig. 10(a). The corresponding loading spectrum showed the signature of albumin.[42] The image reveals a greater concentration of albumin outside the tissue than inside it, as expected.

The second factor [Fig. 10(b)] showed a distribution that we attribute to the ibuprofen–albumin complex; the loading spectrum contained signals due to both components [see pure ibuprofen spectrum in Fig. 10(c)]. The undissolved ibuprofen observed by univariate analysis [FTIR images in Fig. 6(b)] is here depicted at the right-hand edge of the score image [see Fig. 10(b)]. The complex is clearly detected within the tissue [see oval in Fig. 10(b)]; this result could not have been obtained by integration over the original dataset because the absorbance of the ibuprofen bands in the spectra of the tissue was too low.

Figure 10(d) is the transmural concentration plot of the ibuprofen–albumin factor across a horizontal line of the array [see Fig. 10(b)]. The graph shows the presence of the complex in approximately half the overall thickness of the wall.

4 Discussion

We previously used micro ATR–FTIR imaging to examine the location and chemical composition of atherosclerotic lesions in sections of the aortic wall of rabbits that had been fed a cholesterol-enhanced diet.[39,40] The approach, dubbed "chemical photography,"[39,40] gave good discrimination between the composition of the normal and diseased wall and revealed effects of age and dietary L-arginine supplements on the distribution and extent of atherosclerosis. Here, we have demonstrated using sections of the same tissue that ATR–FTIR im-
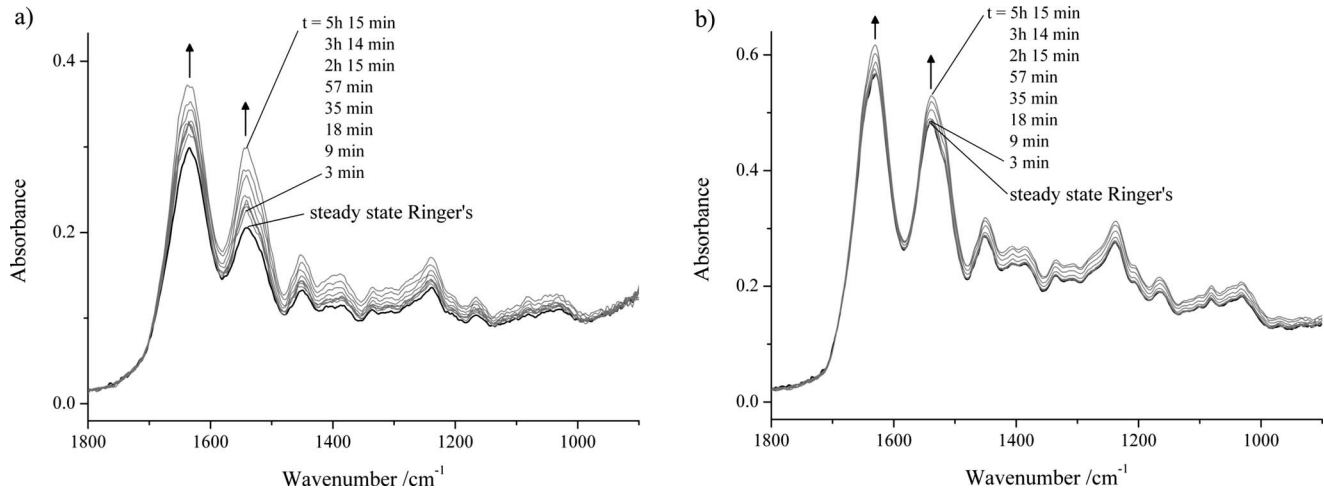
Fig. 7 (a) FTIR spectra extracted from a region within the intima [see asterisk in Fig. 6(a)] at different times after the start of diffusion. The spectrum of the tissue at the steady state without the drug solution is also shown. (b) FTIR spectra extracted from a region within the media [see circle in Fig. 6(a)] at different times of the diffusion. The spectrum of the tissue at steady state without the drug solution is also shown. (The arrows indicate the increase in absorbance of the prominent peptide bands, i.e., amides I and II.)

aging can also be used to assess transport of small and large solutes across the aortic wall. We studied albumin (69 kDa) as an inert model of the macromolecules that play critical roles in the development of atherosclerosis; its concentration profile across the aortic tissue was followed as a function of time. We also studied two model drugs: benzyl nicotinate (relative molecular mass 213 Da) and ibuprofen (206 Da). Benzyl nicotinate is the benzyl ester form of niacin. It is more lipophilic than the parent compound (which lowers circulating lipid levels, is a potent vasodilator, and is frequently used in clinical practice[43,44]) and was employed in the present study because its partitioning into lipid-rich lesions provides a good test of the ability of ATR–FTIR imaging to discriminate between uptake by overtly healthy and diseased tissue. Ibuprofen is a cyclo-oxygenase inhibitor with potent anti-inflammatory effects; recent studies have investigated its influence on experimental atherosclerosis in animals.[45,46] It

was used in the present study because the facilitation of its transport into the wall by albumin provides a good test of the ability of multivariate analysis to increase the discriminatory power of ATR–FTIR imaging.

The image area was $550 \times 610 \ \mu m^2$ and the spatial resolution approximately 15 to 20 μm. The sample depth probed is restricted to few micrometers by the depth of penetration of the evanescent wave into the specimen. This compares favorably with the large number of radiotracer-based studies in which solutes have been detected by counting radioactivity in whole sections of the wall, with typical dimensions on the order of 1 cm $\times$ 1 cm $\times$ 10 μm. Although higher resolutions can theoretically be obtained with radiotracers by using autoradiography, very few such studies have been published; the low uptake of plasma molecules into the wall means that impracticably high concentrations and long exposures are re-
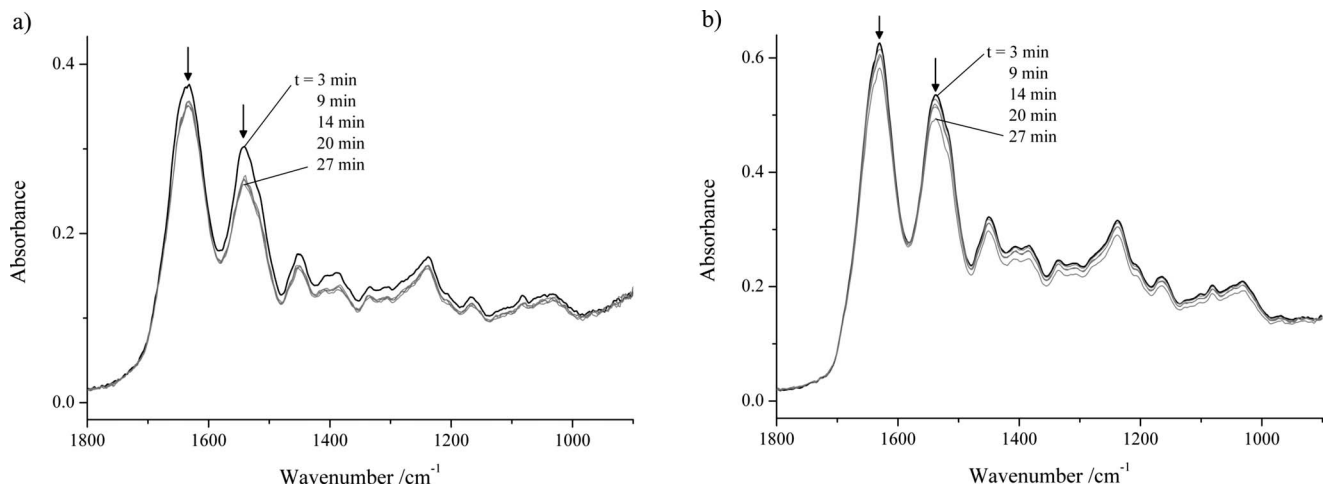

Fig. 8 (a) FTIR spectra extracted from a region within the intima [see asterisk in Fig. 6(a)] at different times after the start reverse diffusion of the drug from the tissue. (b) FTIR spectra extracted from a region within the media [see circle in Fig. 6(a)] at different times after the start of reverse diffusion of the drug from the tissue. (The arrows indicate the decrease in absorbance of the prominent peptide bands, i.e., amides I and II.)
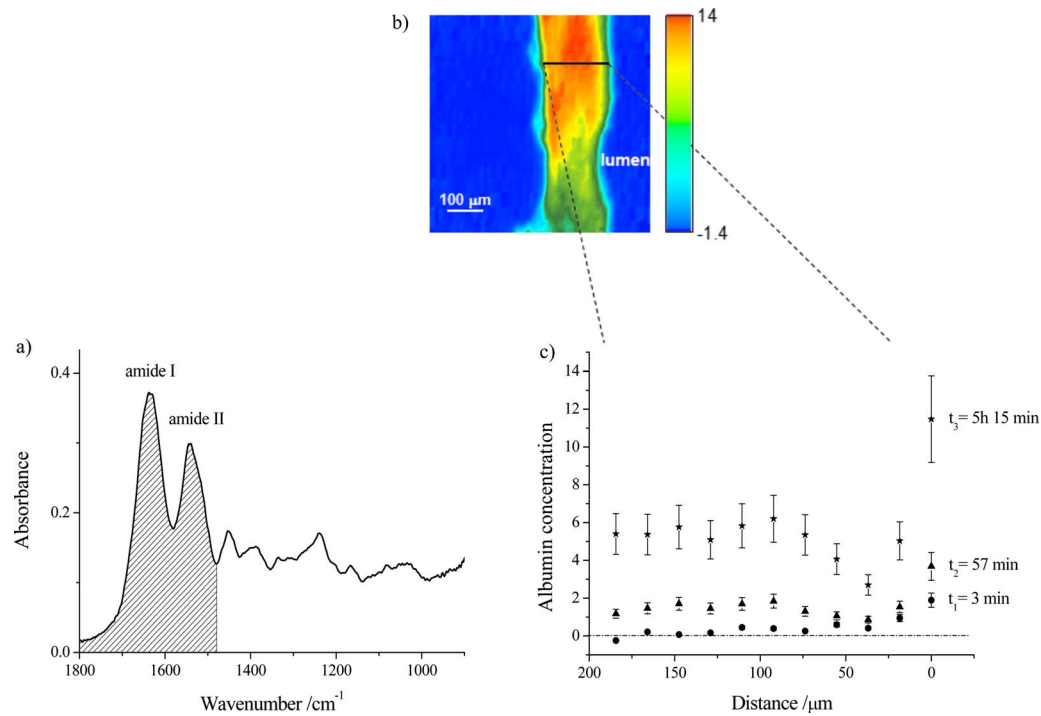
Fig. 9 (a) Integration method applied to derive transmural concentration profiles of albumin across the aortic wall. (b) ATR–FTIR image of the tissue at steady state obtained by integration of the amide II band, in the range 1580 to 1480 cm^{-1}; the line shows the pixels of the image from which FTIR spectra were extracted. (c) Transmural concentration profiles of albumin across the artery wall for different times after the start of diffusion.
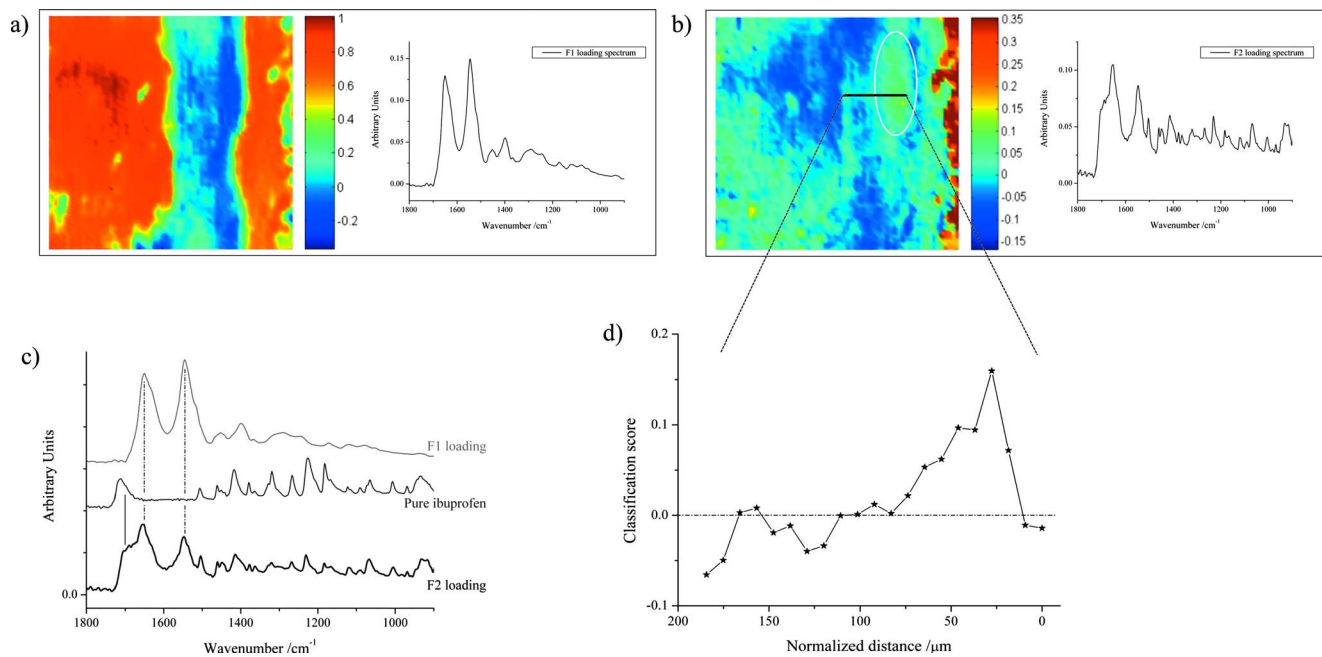

Fig. 10 Results of factor analysis performed on the subtraction image at the end of the ibuprofen–albumin diffusion experiment (time=5 h 15 min). (a) Score image and loading spectrum of the first factor, giving the distribution of albumin in this imaged area. (b) Score image and loading spectrum of the second factor, representing the distribution of ibuprofen–albumin complex. (The oval indicates the region of the tissue showing the occurrence of this complex; the line shows the pixels of the image from which FTIR spectra were extracted.) (c) F1 and F2 loading spectra along with a spectrum of pure ibuprofen (powder). (The dotted and solid lines indicate that the spectral positions of the main FTIR bands are reproduced between the different profiles.) (d) Transmural concentration profile of the ibuprofen–albumin complex across the artery wall at the end of the diffusion experiment.

quired. Since both these radiotracer detection methods destroy the sample, they can be used only at one time point, whereas the ATR–FTIR-based method can follow transport continuously.

Methods employing fluorescence microscopy in conjunction with dye-labeled solutes have somewhat greater resolution than we obtained in the present study. Furthermore, it is possible to make frequent measurements on the same sample[47] so long as care is taken to limit photobleaching of the dye during the repeated exposures to the fluorescence-exciting illumination. However, the need to bind large dye molecules (typically, ~500 kDa) to the solute is a substantial disadvantage; even proteins may be significantly modified by such conjugation,[48] while the size of the label may equal or even exceed that of smaller solutes. ATR–FTIR imaging avoids this problem since its chemical specificity is alone sufficient to discriminate between the solute and tissue sample. An additional advantage arising from this chemical specificity is that mixtures of solutes can be examined and separated. In the present study, for example, we were able to demonstrate that albumin acts as drug carrier[49] for ibuprofen, which was otherwise not observed to enter the aortic wall; factor analysis revealed the presence of an ibuprofen–albumin complex within the artery wall that was undetected by univariate analysis.

A disadvantage of the method used for assessing arterial mass transport in the present study is that no pressure gradient is applied across wall, unlike *in vivo*, where there is a higher pressure inside the vessel lumen than outside. Additionally, the tissue was dead and had been fixed, ruling out the possibility of active or vesicular transport within the endothelial layer. These disadvantages reflect limitations of the specimen handling and mounting procedures, and would be surmountable with suitable apparatus; they do not alter conclusions about the fundamental utility of ATR–FTIR imaging for such studies. Transport of small molecules across the wall *in vivo* is predominantly diffusive and independent of active or vesicular processes within endothelial cells, but the significance of pressure-driven convection and vesicular transport increases for larger solutes. Nevertheless, diffusional, endothelium-independent properties are of interest even for arterial macro-molecular transport (and have been examined with radiotracer techniques[9]), while for vessels not exposed to high luminal pressures (such as veins) and for nonvascular tissues, they are of paramount importance. The *in situ* fixation of the tissue at physiological pressure prevented it from collapsing when excised but will have altered the chemistry of wall components. We previously showed[40] that it has only minor influences on absorbances in the spectral regions examined here; others have shown an absence of effects of fixation on transport properties such as hydraulic conductance of the endothelium[50] and permselectivity of intact vascular beds[51] which may explain why our results are consistent with earlier work employing dead but unfixed tissue.

The fact that ATR–FTIR imaging allows repetitive measurement of the same sample is important because the evolution of concentration profiles across the wall with time provides additional information about transport processes. After short times, when concentrations of solute in the wall are low, uptake depends primarily on the resistance to entry. After several hours, however, an equilibrium is reached, and concen-

trations then depend on the space available for solutes within the wall. Consistent with previous results,[9] we found that at these longer times, concentrations of macromolecules were higher in the inner and outer layers of the wall than in the middle; this phenomenon is thought to reflect a looser packing of the ground substance of the wall in these regions. The packing density is in turn likely to influence the resistance of the different layers to transport across the wall.

5 Conclusions

We have demonstrated that ATR–FTIR imaging allows measurement of the diffusion of small solutes, such as drugs, and macromolecules into the arterial wall *in vitro*. The model drug benzyl nicotinate showed higher affinity for atherosclerotic plaque than for healthy tissue, while ibuprofen required albumin to act as a drug carrier; it was otherwise undetected within the tissue. The presence and distribution of ibuprofen in the artery wall, transported by albumin was demonstrated by multivariate subtraction image analysis. The results were obtained by a chemically specific method, as a function of time with the same specimen, and without labeling the solutes, a unique combination of advantages.

References

1. P. D. Weinberg, "Rate-limiting steps in the development of atherosclerosis: the response-to-influx theory," *J. Vasc. Res.* **41**, 1–17 (2004).
2. M. A. Lovich, M. Philbrook, S. Sawyer, E. Weselcouch, and E. R. Edelman, "Arterial heparin deposition: role of diffusion, convection, and extravascular space," *Am. J. Physiol. Heart Circ. Physiol.* **275**, H2236–H2242 (1998).
3. L. B. Nielsen, "Transfer of low density lipoprotein into the arterial wall and risk of atherosclerosis," *Atherosclerosis* **123**, 1–15 (1996).
4. R. L. Bratzler, G. M. Chisolm, C. K. Colton, K. A. Smith, and R. S. Lees, "Distribution of labeled low-density lipoproteins across rabbit thoracic aorta *in vivo*," *Atherosclerosis* **28**, 289–307 (1977).
5. R. L. Bratzler, G. M. Chisolm, C. K. Colton, K. A. Smith, D. B. Zilversmit, and R. S. Lees, "Distribution of labeled albumin across rabbit thoracic aorta *in vivo*," *Circ. Res.* **40**, 182–190 (1977).
6. G. Meyer, R. Merval, and A. Tedgui, "Effects of pressure-induced stretch and convection on low-density lipoprotein and albumin uptake in the rabbit aortic wall," *Circ. Res.* **79**, 532–540 (1996).
7. R. G. Tompkins, M. L. Yarmush, J. J. Schnitzer, C. K. Colton, K. A. Smith, and M. B. Stemerman, "Low-density lipoprotein transport in blood-vessel walls of squirrel-monkeys," *Am. J. Physiol.* **257**, H452–H464 (1989).
8. M. J. Lever and M. T. Jay, "Albumin and Cr-Edta uptake by systemic arteries, veins, and pulmonary-artery of rabbit," *Atherosclerosis* **10**, 551–558 (1990).
9. C. G. Caro and M. J. Lever, "Effect of vasoactive agents and applied stress on the albumin space of excised rabbit carotid arteries," *Atherosclerosis* **46**, 137–146 (1983).
10. M. S. Penn, M. R. Koelle, S. M. Schwartz, and G. M. Chisolm, "Visualization and quantification of transmural concentration profiles of macromolecules across the arterial-wall," *Prog. Colloid Polym. Sci.* **67**, 11–22 (1990).
11. M. S. Penn, G. M. Saidel, and G. M. Chisolm, "Vascular injury by endotoxin—changes in macromolecular transport parameters in rat aortas invivo," *Am. J. Physiol.* **262**, H1563–H1571 (1992).
12. C. M. Yang and H. A. Burt, "Drug-eluting stents: factors governing local pharmacokinetics," *Adv. Drug Delivery Rev.* **58**, 402–411 (2006).

13. J. M. Lanao and M. A. Fraile, "Drug tissue distribution: study methods and therapeutic implications," *Curr. Pharm. Des.* **11**, 3829–3845 (2005).

14. A. D. Levin, N. Vukmirovic, C. W. Hwang, and E. R. Edelman, "Specific binding to intracellular proteins determines arterial transport properties for rapamycin and paclitaxel," *Proc. Natl. Acad. Sci. U.S.A.* **101**, 9463–9467 (2004).

15. C. J. Creel, M. A. Lovich, and E. R. Edelman, "Arterial paclitaxel distribution and deposition," *Circ. Res.* **86**, 879–884 (2000).

16. C. W. Hwang and E. R. Edelman, "Arterial ultrastructure influences transport of locally delivered drugs," *Circ. Res.* **90**, 826–832 (2002).

17. W. K. Wan, M. A. Lovich, C. W. Hwang, and E. R. Edelman, "Measurement of drug distribution in vascular tissue using quantitative fluorescence microscopy," *J. Pharm. Sci.* **88**, 822–829 (1999).

18. S. G. Kazarian and K. L. A. Chan, "'Chemical photography' of drug release," *Macromolecules* **36**, 9866–9872 (2003).

19. S. G. Kazarian and K. L. A. Chan, "Sampling approaches in Fourier transform infrared imaging applied to polymers," *Prog. Colloid Polym. Sci.* **132**, 1–6 (2006).

20. S. G. Kazarian and K. L. A. Chan, "Applications of ATR-FTIR spectroscopic imaging to biomedical samples," *Biochim. Biophys. Acta* **1758**, 858–867 (2006).

21. M. K. Kuimova, K. L. A. Chan, and S. G. Kazarian, "Chemical imaging of live cancer cells in the natural aqueous environment," *Appl. Spectrosc.* **63**, 164–171 (2009).

22. D. Biswal and J. Z. Hilt, "Microscale analysis of patterning reactions via FTIR imaging: application to intelligent hydrogel systems," *Polymer* **47**, 7355–7360 (2006).

23. M. Boncheva, F. H. Tay, and S. G. Kazarian, "Application of attenuated total reflection Fourier transform infrared imaging and tape-stripping to investigate the three-dimensional distribution of exogenous chemicals and the molecular organization in *Stratum corneum*," *J. Biomed. Opt.* **13**, 064009 (2008).

24. K. L. A. Chan and S. G. Kazarian, "Chemical imaging of the stratum corneum under controlled humidity with the attenuated total reflection Fourier transform infrared spectroscopy method," *J. Biomed. Opt.* **12**, 044010 (2007).

25. S. G. Kazarian, "Enhancing high-throughput technology and microfluidics with FTIR spectroscopic imaging," *Anal. Bioanal. Chem.* **388**, 529–532 (2007).

26. J. L. Koenig and J. P. Bobiak, "Raman and infrared imaging of dynamic polymer systems," *Macromol. Mater. Eng.* **292**, 801–816 (2007).

27. R. Mendelsohn, H. C. Chen, M. E. Rerek, and D. J. Moore, "Infrared microspectroscopic imaging maps the spatial distribution of exogenous molecules in skin," *J. Biomed. Opt.* **8**, 185–190 (2003).

28. T. Chen, M. J. Lee, Y. S. Kim, S. Lee, S. Kummar, M. Gutierrez, S. M. Hewitt, J. B. Trepel, and I. W. Levin, "Pharmacodynamic assessment of histone deacetylase inhibitors: infrared vibrational spectroscopic imaging of protein acetylation," *Anal. Chem.* **80**, 6390–6396 (2008).

29. C. Ricci, S. Bleay, and S. G. Kazarian, "Spectroscopic imaging of latent fingermarks collected with the aid of a gelatin tape," *Anal. Chem.* **79**, 5771–5776 (2007).

30. M. Romeo, B. Mohlenhoff, M. Jennings and M. Diem, "Infrared micro-spectroscopic studies of epithelial cells," *Biochim. Biophys. Acta* **1758**, 915–922 (2006).

31. R. Salzer, G. Steiner, H. H. Mantsch, J. Mansfield, and E. N. Lewis, "Infrared and Raman imaging of biological and biomimetic samples," *Fresenius' J. Anal. Chem.* **366**, 712–726 (2000).

32. S. G. Kazarian and J. van der Weerd, "Simultaneous FTIR spectroscopic imaging and visible photography to monitor tablet dissolution and drug release," *Pharm. Res.* **25**, 853–860 (2008).

33. J. Koenig, "FTIR imaging of polymer dissolution," *Adv. Mater.* **14**, 457-460 (2002).

34. B. A. Miller-Chou and J. L. Koenig, "A review of polymer dissolution," *Prog. Polym. Sci.* **28**, 1223–1270 (2003).

35. J. van der Weerd and S. G. Kazarian, "Combined approach of FTIR imaging and conventional dissolution tests applied to drug release," *J. Controlled Release* **98**, 295–305 (2004).

36. A. Gupper and S. G. Kazarian, "Study of solvent diffusion and solvent-induced crystallization in syndiotactic polystyrene using FT-IR spectroscopy and imaging," *Macromolecules* **38**, 2327–2332 (2005).

37. K. L. A. Chan, F. H. Tay, C. Taylor, and S. G. Kazarian, "A novel approach for study of *in situ* diffusion in human hair using Fourier transform infrared spectroscopic imaging," *Appl. Spectrosc.* **62**, 1041–1044 (2008).

38. J. Van der Weerd and S. G. Kazarian, "Release of poorly soluble drugs from HPMC tablets studied by FTIR imaging and flow-through dissolution tests," *J. Pharm. Sci.* **94**, 2096–2109 (2005).

39. C. S. Colley, S. G. Kazarian, P. D. Weinberg, and M. J. Lever, "Spectroscopic imaging of arteries and atherosclerotic plaques," *Biopolymers* **74**, 328–335 (2004).

40. F. Palombo, S. G. Cremers, P. D. Weinberg, and S. G. Kazarian, "Application of Fourier transform infrared spectroscopic imaging to the study of effects of age and dietary l-arginine on aortic lesion composition in cholesterol-fed rabbits," *J. R. Soc., Interface* **6**, 669–680 (2009).

41. K. L. A. Chan, F. H. Tay, G. Poulter, and S. G. Kazarian, "Chemical imaging with variable angles of incidence using a diamond attenuated total reflection accessory," *Appl. Spectrosc.* **62**, 1102–1107 (2008).

42. S. L. Wang, Y. S. Wei, and S. Y. Lin, "Subtractive similarity method used to study the infrared spectra of proteins in aqueous solution," *Vib. Spectrosc.* **31**, 313–319 (2003).

43. J. M. Andanson, J. Hadgraft, and S. G. Kazarian, "*In situ* permeation study of drug through the *stratum corneum* using ATR-FTIR spectroscopic imaging," *J. Biomed. Opt.* **14**, 034011 (2009).

44. S. L. Airan-Javia, R. L. Wolf, M. L. Wolfe, M. Tadesse, E. Mohler, and M. P. Reilly, "Atheroprotective lipoprotein effects of a niacin-simvastatin combination compared to low- and high-dose simvastatin monotherapy," *Am. Heart J.* **157**, 687.e1–688.e8 (2009).

45. B. Sekalskaa, A. Ciechanowiczb, B. Dolegowskac, and M. Naruszewiczd, "Effect of ibuprofen on the development of fat-induced atherosclerosis in New Zealand rabbits," *J. Exp. Anim. Sci.* **43**, 283–299 (2007).

46. J. K. Dabhi, J. K. Solanki, and A. Mehta, "Antiatherosclerotic activity of ibuprofen, a nonselective COX inhibitor—an animal study," *J. Exp. Biol.* **46**, 476–481 (2008).

47. K. H. Parker and C. P. Winlove, "Measurement of diffusion coefficients in biopolymer solutions and gels," in *Methods in Cartilage Research*, A. Maroudas and K. Kuettner, Eds., pp. 255–258, Academic Press, London (1990).

48. R. C. Nairn, *Fluorescent Protein Tracing*, Churchill Livingstone, Edinburgh (1976).

49. M. A. Lovich, C. Creel, K. Hong, C. W. Hwang, and E. R. Edelman, "Carrier proteins determine local pharmacokinetics and arterial distribution of paclitaxel," *J. Pharm. Sci.* **90**, 1324–1335 (2001).

50. M. R. Turner, "Flows of liquid and electrical current through monolayers of cultured bovine arterial endothelium," *J. Physiol. (London)* **449**, 1–20 (1992).

51. B. Haraldsson and B. R. Johansson, "Changes in transcapillary exchange induced by perfusion fixation with glutaraldehyde, followed by measurements of capillary filtration coefficient, diffusion capacity and albumin clearance," *Acta Physiol. Scand.* **124**, 99–106 (1985).